

# CTF RESIDUAL FORMULATION OF SOLID LIQUID COUPLING

C. Dances<sup>1</sup>, V. Mousseau<sup>2</sup> and M. Avramova<sup>1</sup>

<sup>1</sup>: Department of Mechanical and Nuclear Engineering, The Pennsylvania State University, 137 Reber Building, University Park, PA 16802, USA

<sup>2</sup>: Computer Science Research Institute, Sandia National Labs, 1450 Innovation Parkway, Albuquerque, NM 87123, USA  
[cad39@psu.edu](mailto:cad39@psu.edu), [vamouss@sandia.gov](mailto:vamouss@sandia.gov), [mna109@psu.edu](mailto:mna109@psu.edu)

## ABSTRACT

Nuclear engineering codes are being used to simulate more challenging problems and at higher fidelities than they were initially developed for. In order to expand the capabilities of these codes, state of the art numerical methods and computer science need to be implemented. One of the key players in this effort is the Consortium for Advanced Simulation of Light Water Reactors (CASL) through development of the Virtual Environment for Reactor Applications (VERA). The sub-channel thermal hydraulic code used in VERA, COBRA-TF (Coolant-Boiling in Rod Arrays - Three Fluids), is partially developed at the Pennsylvania State University by the Reactor Dynamics and Fuel Management Research Group (RDFMG). The RDFMG version COBRA-TF is referred to as CTF.

In an effort to help meet the objectives of CASL, a version of CTF has been developed that solves the residual formulation of the one-dimensional single-phase conservation equations. The formulation of the base equations as residuals allows the code to be run semi-implicitly or fully implicitly while clearly defining the original conservation equations. This paper outlines work to integrate one dimensional solid conduction equations into the residual formulation. This allows the coupling between the solid and liquid equations to be either explicit or implicit. A simple test problem consisting of a single liquid channel and fuel pin is used to compare the different numerical models available from the new residual formulation to an analytical solution. The methods are compared both for steady state and transient conditions to quantify the accuracy of each method. The ability to choose appropriate numerical methods allows for greater fidelity and decreases computational expenses. The comparison to an analytical solution helps to verify that the code is working properly.

## KEYWORDS

CTF, Thermal Hydraulic, Residual, Jacobian, Solid Liquid Coupling

## 1. INTRODUCTION

For the past several decades, the primary focus in nuclear engineering within the United States has been on light water reactors (LWR). Commercially, all nuclear reactors are either boiling water reactors (BWR) or pressurized water reactors (PWR). Correct computation of the thermal hydraulics within the reactor core leads to efficient design and accuracy in the safety analysis. A popular subchannel code for modeling the hydrodynamics within the reactor core is CTF, which is a subchannel thermal-hydraulics code developed from COBRA-TF [1]. This FORTRAN based code solves 8 conservation equations for liquid, entrained droplet, and vapor phases, plus one conservation equation for non-condensable gases. A residual formulation of the code has been created that is able to solve the 1-D single-phase fluid solution. While other residual formulations have been formed for various versions of CTF [2], none have been integrated into the CASL version of CTF. This paper outlines the initial work in coupling the liquid and solid solutions for the residual formulation. Explicit and implicit coupling between the solid and liquid solutions are considered for transient and steady state problems. The steady state calculations are compared to the analytical solution for accuracy.

## 2. CTF

The thermal hydraulics of a LWR core is an important part of nuclear reactor design. CTF has the ability to solve for the temperature and pressure of water within the rod structure of a LWR reactor core. Currently, the conservation equations analytically reduce into a pressure matrix in a semi-implicit method in which rod temperatures are solved for explicitly. The residual formulation of the code currently solves the 1-D axial single-phase liquid and 1-D radial solid energy conservation. This residual formulation allows for greater flexibility in the selection of the numerical methods as well as easy parameter exposure work.

### 2.1. 1-D Single Phase Liquid Conservation Equations

For the single-phase formulation of the Euler equations, the unknown variables are pressure  $P$ , velocity  $u$ , enthalpy  $h$ , and density  $\rho$ . Density is considered a function of pressure and enthalpy according to the equation of state as dictated by the steam tables [3]. To solve for the remaining three variables, three conservation equations are needed. The conservation of mass given in equation 1 is the most basic in which the rate of change in density is equal to the advection from the upwinded cell. The conservation of momentum in equation 2 balances the time rate of change of momentum, the advection of momentum from adjacent cells, the gradient of pressure, and body forces. Frictional losses due to grid spacers and other affects are assumed to be zero for the scope of this work in order focus on the solid liquid coupling. The conservation of energy in equation 3 contains two temporal terms: the time rate of change of the enthalpy and the time rate of change of the pressure. These temporal terms are balanced against the advection of the enthalpy. The amount of heat entering the channel is calculated as  $h_f(T_w - T_l)$ , where  $h_f$  is the heat transfer coefficient from the single phase Dittus-Boelter [4] correlation,  $T_w$  is the wall temperature, and  $T_l$  is the bulk liquid temperature of the cell.

$$\frac{\partial \rho}{\partial t} + \frac{\partial \rho u}{\partial x} = 0 \quad (1)$$

$$\frac{\partial u}{\partial t} + u \frac{\partial u}{\partial x} + \frac{1}{\rho} \frac{\partial P}{\partial x} + g = 0 \quad (2)$$

$$\rho \frac{\partial h}{\partial t} + h \frac{\partial \rho}{\partial t} - \frac{\partial P}{\partial t} + \rho u \frac{\partial h}{\partial x} + h \frac{\partial \rho u}{\partial x} - \frac{q_{rod}}{v_{lq}} = 0 \quad (3)$$

### 2.1.1. CTF fluid meshing

The finite volume structure in CTF in Figure 1 is for a one-dimensional channel in the axial direction with  $n$  number of cells. The first and last cells, 0 and  $n + 1$ , respectively, are ghost cells that act as the boundary conditions for the problem. Pressure, enthalpy, and density are averaged over the cell volume and are located at the center of the cell. Mass flow rate and velocity are located at the faces in between cells. The cells are represented with an index  $i$ , and the faces with indexes of  $i+1/2$  or  $i-1/2$ . This project focuses on this 1D configuration and does not take into account adjacent subchannels.

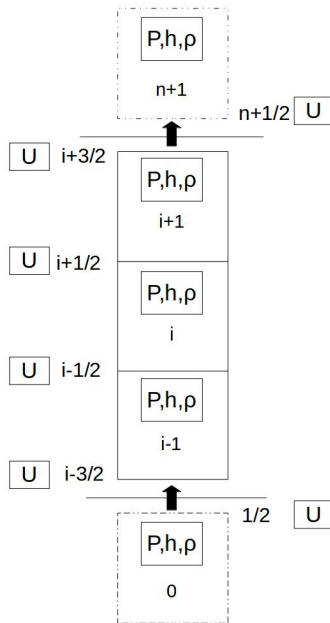


**Figure 1. CTF Fluid Volume Meshing**

### 2.1.2. Fluid finite difference equations

The semi-implicit finite difference formulation of the conservation of mass in equation 4 uses a first order accurate forward differencing method for the temporal derivative and the spatial derivatives. The densities evaluated at momentum indices such as  $i + \frac{1}{2}$  represent the density in the adjacent cell to the momentum surface at  $i + \frac{1}{2}$  in direction opposite the direction of velocity at the momentum position. In this way, the density is always grabbed from upwind from the momentum surface and never downwind. This is necessary because velocity is not affected by changes downwind. For the scope of this project, velocity is always positive, so at momentum cell  $i + \frac{1}{2}$  the density would be evaluated at cell  $i$ . The iterator  $k$ , is the iteration level of the solution. If the solution method is semi-implicit then the number of iterations is one and  $k$  is equal to  $n$ . If the solution method is implicit, then multiple iterations occur until  $k$  increments from  $n$  to  $n + 1$ . The finite difference formulations of the conservation of momentum in equation 5 and the fluid energy conservation in equation 6 are first order accurate for the temporal and spatial derivatives. The last term in the equation is difference between the wall temperature and the bulk fluid temperature times the heat transfer coefficient and the wetted perimeter of the connected rod divided by

the fluid cell area. This numerator of this term is also present in the solid conduction equations and is responsible for coupling the solid energy equations to the fluid energy equations. When the fluid equations are solved for semi-implicitly, all of these evaluated at the current time step  $n$ , and the solid conduction equations are explicitly coupled to the fluid equations. When the fluid equations are solved for implicitly, the wall temperature and heat transfer coefficient are solved for at the next time size. The fluid equations are then implicitly coupled to the solid equations.

$$\frac{\rho_i^{n+1} - \rho_i^n}{\Delta t} + \frac{\rho_{i+\frac{1}{2}}^k u_{i+\frac{1}{2}}^{n+1} - \rho_{i-\frac{1}{2}}^k u_{i-\frac{1}{2}}^{n+1}}{\Delta x} = 0 \quad (4)$$

$$\frac{u_{i+\frac{1}{2}}^{n+1} - u_{i+\frac{1}{2}}^n}{\nabla t} + u_{i+\frac{1}{2}}^k \frac{u_{i+\frac{1}{2}}^{n+1} - u_{i-\frac{1}{2}}^k}{\Delta x} + \frac{1}{\bar{\rho}_{i+\frac{1}{2}}^k} \frac{P_{i+1}^{n+1} - P_i^{n+1}}{\Delta x} + g = 0 \quad (5)$$

$$\rho_i^k \frac{h_i^{n+1} - h_i^n}{\Delta t} + h_i^k \frac{\rho_i^{n+1} - \rho_i^n}{\Delta t} - \frac{P_i^{n+1} - P_i^n}{\Delta t} + \rho_i^k u_{i+\frac{1}{2}}^{n+1} \frac{h_i^{n+1} - h_{i-1}^{n+1}}{\Delta x} + h_i^k \frac{\rho_{i+\frac{1}{2}}^k u_{i+\frac{1}{2}}^{n+1} - \rho_{i-\frac{1}{2}}^k u_{i-\frac{1}{2}}^{n+1}}{\Delta x} - \frac{2\pi r_{co} h_l (T_i^{n+1} - T_f)}{A_{liq}} = 0 \quad (6)$$

## 2.2. 1-D Radial Solid Conduction Equation

The conduction equation for a cylindrical system is given in equation 7. The first term represents the amount of energy stored within the solid area within a unit time. The second term is the conduction in the radial direction. The second and third terms are the conduction in the azimuthal and axial directions, respectively. The last term represents the heat generation within the solid.

$$\rho c_p \frac{\partial T}{\partial t} - \frac{1}{r} \frac{\partial}{\partial r} \left( kr \frac{\partial T}{\partial r} \right) - \frac{1}{r^2} \frac{\partial}{\partial \theta} \left( k \frac{\partial T}{\partial \theta} \right) - \frac{\partial}{\partial z} \left( k \frac{\partial T}{\partial z} \right) - q''' = 0 \quad (7)$$

This work focuses on the 1D radial equations setting the derivatives with respect to the angular and axial directions to zero. Equation 7 now reduces to equation 8.

$$\rho c_p \frac{\partial T}{\partial t} - \frac{1}{r} \frac{\partial}{\partial r} \left( kr \frac{\partial T}{\partial r} \right) - q''' = 0 \quad (8)$$

When the radius is zero, the fuel temperature is considered to be a maximum giving the boundary condition in equation 9.

$$\left( \frac{\partial T}{\partial r} \right)_{r=0} = 0 \quad (9)$$

### 2.2.1. CTF rod meshing

The nuclear rod geometry types in CTF are meshed at each axial level according to figure 2 where the red region is fuel and the grey region is cladding. The black dots represent the nodes within the fuel. Each node covers a region within the rod as bounded by the dashed lines. The nodes within the fuel are located at the center of the region. Each region is assumed to have uniform properties with values evaluated at the node. The last node within the fuel is located at the surface of the fuel at the interface with the gap. There are two additional nodes that represent the outer clad surface and the inner clad surface respectively. The gap between the outer surface of the fuel and the inner surface of the cladding has a specified heat transfer coefficient or is calculated using the dynamic gap conductance model.

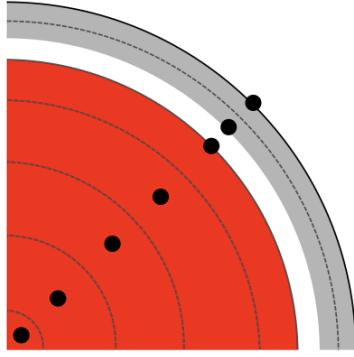


**Figure 2. Radial Rod Meshing**

The outer surface of the cladding is assumed to be in contact with the fluid in the adjacent channel on that axial level. The rods have the same number of axial levels as the fluid, but do not have ghost cells at the top and bottom. Instead the first and last fluid axial levels are connected to two rod axial levels as shown by Figure 3, where the rod axial levels are on the left, and the fluid axial levels are on the right. The light blue cells are the fluid ghost cells.

		jabs=7
jht=7		jabs=6
jht=6		
jht=5		jabs=5
jht=4		jabs=4
jht=3		jabs=3
jht=2		jabs=2
jht=1		
		jabs=1

**Figure 3. Radial Rod Meshing**

### 2.2.2. Solid finite difference equations

The conduction equation can be approximated using the finite difference method, or the control volume difference method [5]. The control volume method will be used since it is the same method utilized in the original version of CTF. The implicit finite difference equation now looks like equation 10.

$$\rho_{fuel} c_{p,fuel} \frac{T_i^{n+1} - T_i^n}{\Delta t} - \frac{2\pi}{A_i} \left( k_{f,i+\frac{1}{2}} r_{i+\frac{1}{2}} \left( \frac{T_{i+1}^{n+1} - T_i^{n+1}}{\Delta r_{i+1}} \right) - k_{f,i-\frac{1}{2}} r_{i-\frac{1}{2}} \left( \frac{T_i^{n+1} - T_{i-1}^{n+1}}{\Delta r_{i-1}} \right) \right) - q''' = 0 \quad (10)$$

The density on the temporal term is defined as the cold mass of the node divided by the current volume of the node, so that mass is not lost in the presence of expansion. The temporal derivative is approximated with first order accurate forward differencing. The spatial derivatives are evaluated at the right

boundary,  $i + \frac{1}{2}$ , and the left boundary,  $i - \frac{1}{2}$ , using first order forward differencing. When  $i = 1$  at the inner most node, the radius at the left boundary and the derivative of the temperature is zero. At the boundary between the surface of the fuel and the inside surface of the cladding, a different set of finite difference equations are needed as given by equation 11. The fuel spatial derivatives now use backward differencing since there is no fuel in the forward direction. The volumetric heat rate across the gap can be calculated as the heat flux across the gap times the perimeter of the boundary divided by the area of the region. The heat flux across the gap is evaluated as the difference between the cladding inner surface temperature and the fuel outer surface temperature times the heat transfer coefficient of the gap.

$$\rho_{fuel} c_{p,fuel} \frac{T_i^{n+1} - T_i^n}{\Delta t} + \frac{2\pi}{A_i} \left( k_{f,i-\frac{1}{2}} r_{i-\frac{1}{2}} \left( \frac{T_i^{n+1} - T_{i-1}^{n+1}}{\Delta r_{i-1}} \right) \right) - q''' - \frac{2\pi r_i h_{gap}}{A_i} (T_{i+1}^{n+1} - T_i^{n+1}) = 0 \quad (11)$$

The finite difference equation between the inner and outer cladding surfaces given by equation 13 has no heat generation or conduction from the fuel. Instead the volumetric heat rate is calculated using the term for the volumetric heat rate across the gap and a similar term but for the volumetric heat rate across the cladding. Since the cladding does not have any heat generation, this term is represented as the temperature difference across the cladding times the thermal resistance across the cladding times the perimeter of the cladding divided by the area of the inner cladding region.

$$\rho_{clad} c_{p,clad} \frac{T_i^{n+1} - T_i^n}{\Delta t} + \frac{2\pi r_i h_{gap}}{A_i} (T_{i+1}^{n+1} - T_i^{n+1}) - \frac{2\pi}{A_i} \left( k_{c,i+\frac{1}{2}} r_{i+\frac{1}{2}} \left( \frac{T_{i+1}^{n+1} - T_i^{n+1}}{\Delta r_{i+1}} \right) \right) = 0 \quad (13)$$

The finite difference equation between the inner and outer cladding surfaces given by equation 14 relates the wall temperature to the bulk fluid temperature at the same axial level. The volumetric heat rate lost to the fluid is represented as the temperature difference between the wall and the fluid times the thermal resistance of the fluid and divided by the outer cladding region.

$$\rho_{clad} c_{p,clad} \frac{T_i^{n+1} - T_i^n}{\Delta t} + \frac{2\pi}{A_i} \left( k_{i-\frac{1}{2}} r_{i-\frac{1}{2}} \left( \frac{T_i^{n+1} - T_{i-1}^{n+1}}{\Delta r_{i-1}} \right) \right) - \frac{2\pi r_{co}}{A_i} h_l (T_i^{n+1} - T_f) = 0 \quad (14)$$

The numerator in the last term is also in the fluid energy conservation equation. The heat transfer coefficient is currently calculated using the Dittus-Boelter correlation. The fluid properties are evaluated at the bulk fluid temperature. When the fluid finite equations are solved for implicitly, they will impact the solid conduction equations through the calculation of the heat transfer coefficient and the fluid temperature.

### 2.3. Residual Formulation and Jacobian Construction

A residual is simply the difference between the value at some future iteration  $k + 1$  and the value at the current iteration  $k$ . Currently in CTF, the future iteration is taken to be the next time step  $n+1$  and the current iteration is the current time  $n$ . The residual can be expressed for desired variables or conservation equations. For example, the residual for density,  $\rho_i$ , is the difference between iterates levels  $k+1$  and  $k$ ,  $\rho_i^{k+1} - \rho_i^k$ . The residuals for the equations are determined by substituting the residuals into the discretized equations, which should effectively change all  $n+1$  into  $k$ . Each cell will have three fluid residual variables and three residual equations. For the entire solution, we will then have a residual variable array  $\delta X$ , and a residual function array  $F(X)$  which defines a linear system  $J\delta X = F(X)$ . The Jacobian matrix is defined as the derivative of each response of the function  $F_j$  with respect to each variable  $X_i$ . The derivative can be calculated numerically as shown by equation 15 where  $\epsilon$  is a small numerical value.

$$J_{i,j} = \frac{\delta F_j(X_i)}{\delta X_i} \approx \frac{F_j(X_i + \epsilon) - F_j(X_i)}{\epsilon} \quad (15)$$

To build the Jacobian matrix, an object oriented class was created that contains three arrays; an array that points to the residual functions, an array that points to the position within a target variable array, and an array that has the index that the function is to be evaluated at. These lists can be appended in any order, but they have to be appended simultaneously such that variables and functions correspond with each other. The residual function and residual variable arrays can be iterated in nested loops to numerically build the Jacobian matrix where each column represents an index of a residual variable and each row represents a residual function. The explicitly coupled solid liquid Jacobian matrix can be seen on the left in Figure 4, where blue values represent negative entries and red values positive entries. The black lines were drawn on top of the image to represent artificial boundaries between the liquid Jacobian matrix in the top left corner and the solid Jacobian matrix in the top right corner.

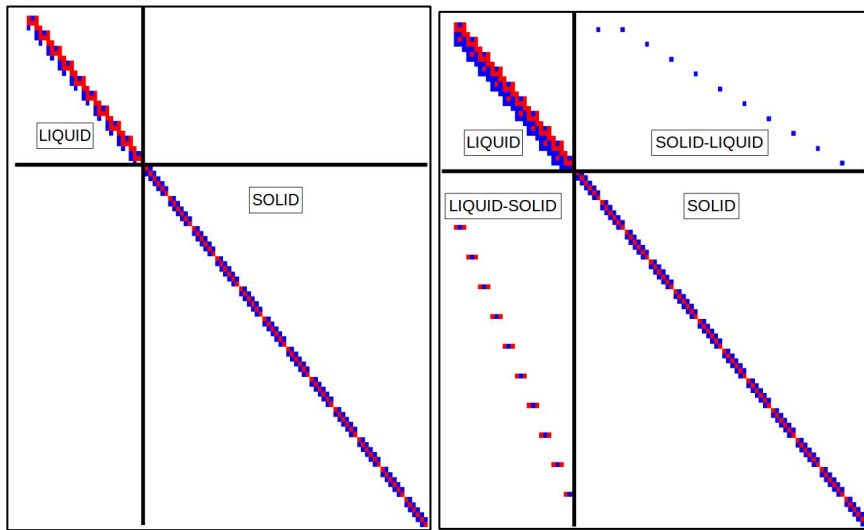


**Figure 4. Explicitly (left) and Implicitly Coupled (right) Liquid Solid Jacobian Matrix**

The fluid Jacobian matrix contains 3 conservation equations for every axial level. The liquid function residuals are appended in the order of mass conservation, energy conservation, and momentum conservation for each axial level. These correspond the pressure, enthalpy, and velocity at each axial level. The liquid Jacobian matrix can be evaluated as either semi-implicit or fully implicit. The solid Jacobian matrix contains 1 energy conservation equation for each node in the rod. Since axial and azimuthal conduction are not computed, each radial level is computed separately from the rest. This can be seen by the lack of cross terms in the Jacobian matrix at each axial level. The Jacobian matrix on the right is an implicit coupling between the implicit liquid Jacobian matrix and the implicit solid matrix. The cross terms in the top right corner represent the effect of the wall temperature on the energy equation in the liquid Jacobian matrix. The terms on the bottom left represent the effects of pressure, enthalpy, and velocity on the energy equation in the solid Jacobian matrix. The implicit matrix is unconditionally stable, allowing for time steps greater than the material Courant limits. Once the coupled Jacobian matrix is constructed, it is solved using the linear Krylov solver from PETSC. The residuals for each of the conservation equations are then L2 normalized over the domain to determine the convergence of the system.

### 3. UNIROM HEATING TEST PROBLEM

#### 3.1. Problem Description

The test problem is a nuclear rod with uniform heat generation with parameters given in Table I. The fuel and cladding are assumed to have constant material properties. The mass flow rate, reference pressure, and inlet temperature approximate normal PWR operating conditions. However, the heat generation rate is much less than normal PWR operating conditions to ensure that the problem remains well within the single-phase regime with an expected outlet temperature of 300.0 °C. Additionally, the problem is set up so that the calculation of the heat transfer coefficient using the Dittus-Boelter correlation is appropriate.

**Table I. Problem Parameters**

Variable	Symbol	Value	Units
Mass Flow Rate	$\dot{m}$	0.300	kg/sec
Reference Pressure	$P_{ref}$	16.50	MPa
Liquid Inlet Temperature	$T_{inlet}$	290.0	°C
Heat Generation Rate	$q'$	4.0	W/m
Active Fuel Length	$L$	3.658	m
Fuel Radius	$r_{fuel}$	0.4096	cm
Outer Cladding Radius	$r_{co}$	0.475	cm
Inner Cladding Radius	$r_{ci}$	0.4174	cm
Rod Pitch	$p$	12.60	cm
Clad Specific Heat Capacity	$C_{p,clad}$	0.431	kJ/kg-K
Clad Density	$\rho_{clad}$	8470.57	kg/m^3
Clad Thermal Conductivity	$k_{clad}$	14.83	W/m-k
Fuel Specific Heat Capacity	$C_{p,fuel}$	0.289	kJ/kg-K
Fuel Density	$\rho_{fuel}$	10970.40	kg/m^3
Fuel Thermal Conductivity	$k_{fuel}$	14.83	W/m-k
Gap Heat Transfer Coefficient	$h_{gap}$	5678.30	kW/m^2-K

#### 3.2. Steady State Analytical Solution

At steady state conditions and for uniform heat generation, the original conduction equation can be integrated to obtain equation 16.

$$T(r, z) - T(r_{fuel}, z) = \frac{q''' r_{fuel}^2}{4 k_{fuel}} \left( 1 - \frac{r^2}{r_{fuel}^2} \right) \quad (16)$$

The temperature at the fuel surface can be calculated from the cladding inner surface temperature and the thermal resistance across the gap as given in equation 17.

$$T(r_{fuel}, z) - T(r_{ci}, z) = \frac{q'}{2\pi r_{ci} h_{gap}} \quad (17)$$

The temperature at the inner surface of the cladding can be calculated from the cladding inner surface temperature and the thermal resistance across the cladding as given by equation 18.

$$T(r_{ci}, z) - T(r_{co}, z) = \frac{q'}{2\pi k_{clad}} \quad (18)$$

The temperature at the outer surface of the cladding can be calculated from the fluid temperature and the thermal resistance due to convection as given by equation 19.

$$T(r_{co}, z) - T_l(z) = \frac{q'}{2\pi r_{co} h_l} \quad (19)$$

Notice that the difference between any radial temperature and the fluid temperature at the same axial level are independent of the axial levels height. This difference will be compared first to verify that the conduction equation is working properly.

### 3.3. Steady State Results

The temperature distribution within the fuel rod relative to the wall surface temperature can be seen in Figure 5. The analytical solution matches well with the different solution methods both within the fuel and at the cladding surfaces. The difference between the analytical solution and the numerical solutions are highest at the fuel centerline. This error is due to the numerical error from the finite differencing approximations made within the fuel. The fuel centerline temperature is extrapolated from the first and second nodal temperatures using a second order accurate forward differencing approximation of the boundary condition in equation 9. Normally CTF uses a different extrapolation method, but to consistently compare to the residual formulation was not used.

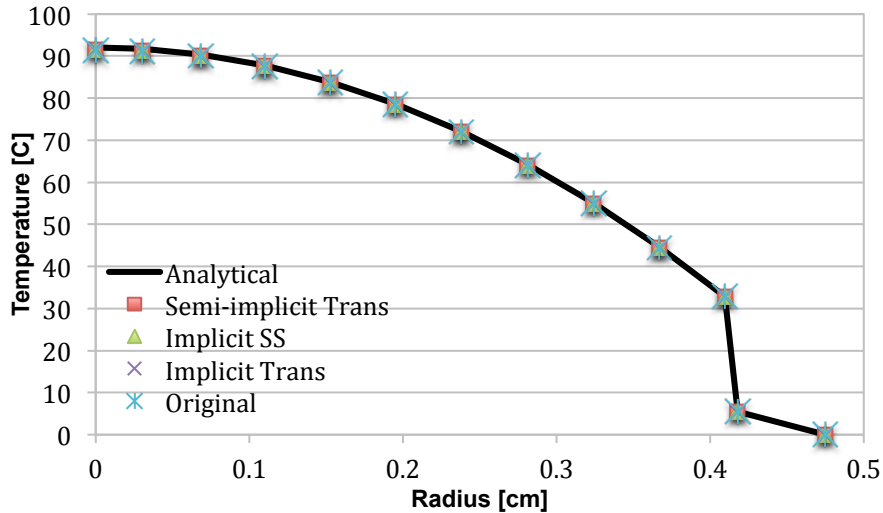


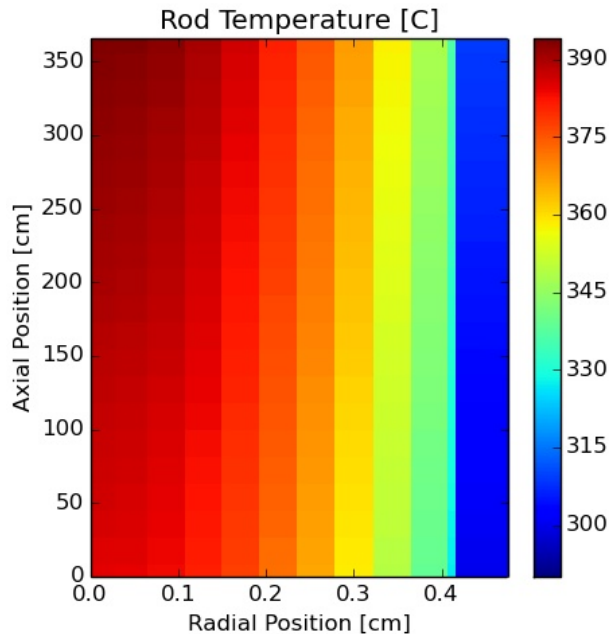
Figure 5. Steady State Radial Temperature Distribution Difference to Rod Surface Temperature

The relative error given in Table II is shown to scale with the inverse of the number of radial nodes in the fuel. The relative error does not scale with heat flux, but the temperature gradient from the fuel centerline to the rod wall does. The numerical error will also change for non-uniform heating and variable material properties within the fuel. The implicit transient solution method has slightly higher numerical error than the semi-implicit transient and implicit steady state solution methods. However, all three residual formulation methods have lower numerical error compared to the original steady state method from CTF. The order of accuracy is difficult to compute, since CTF uses non-uniform meshing near the rod center and since the fuel centerline temperature is extrapolated using a second order accurate method. The non-uniform mesh size also means that a Richardson extrapolation is not valid.

**Table II. Relative Error of Difference Between Fuel Centerline to Rod Surface Temperature**

Radial Nodes in Fuel	Semi-implicit Transient	Implicit Transient	Implicit Steady State	Original Steady State
5	1.33%	1.35%	1.32%	2.15%
10	0.45%	0.48%	0.45%	0.78%
20	0.15%	0.18%	0.14%	0.20%

While there is no solid conduction in the axial direction, the fluid will have a temperature gradient in the axial direction. This will cause a 2-D temperature distribution as shown by Figure 6. The fluid temperature only changes by about 10 C from the inlet to the outlet, but the fuel temperature changes by about 90 C from the outer surface of the cladding to the fuel centerline temperature. The hottest location of the fuel is located on the centerline at the top of the rod. The centerline fuel temperature is slightly under predicted by both the residual formulation and the original versions of CTF. However as table II shows, this is attributable to numerical error.

**Figure 6. Steady State Axial and Radial Temperature Distribution in the Fuel Rod**

### 3.4. Transient Results

The transient simulations were run for 30.0 seconds to reach a pseudo-steady state condition. The rate of change of the temperatures have reached near steady state conditions as shown by Figure 7 were the red lines are fuel node temperatures, and the black lines are cladding node temperatures. The semi-implicit method is used on the left, and the fully implicit method is on the right. For the semi-implicit solution method, a maximum time step size of 0.02 sec was needed to ensure stability. For the implicit solution method time step sizes well over 0.2 seconds could be taken. For the data in the figure, time steps of 1.0 second were used. The implicit Jacobian matrix is stiffer than the Jacobian matrix for the semi-implicit method and therefore takes longer to solve. Additionally, for time steps with large residuals multiple up to 5 iterations are needed. However the advantage of being able to take significantly longer time steps makes up for the increased computational cost per time step required by the semi-implicit method. The temperatures gained from the semi-implicit method and the implicit methods do not differ by significant amounts.

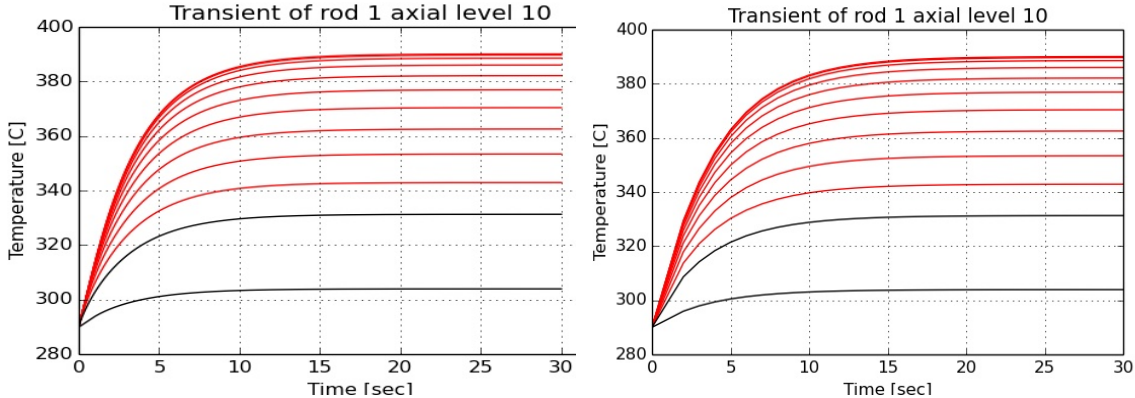


**Figure 7. Plot of the Radial Nodal Temperatures for Semi-Implicit (left) and Implicit (right)**

The transient behavior of temperature profile is shown in Figure 8 where the flat green line is the initial condition, the red line is the final profile, and the black lines are intermediate time steps. It is easier to observe the difference in the number of time steps between the semi-implicit method on the left and the implicit method on the right. The intermediary time steps are still the same, as is the final solution. However, the implicit method will have greater numerical error compared to the semi-implicit method.

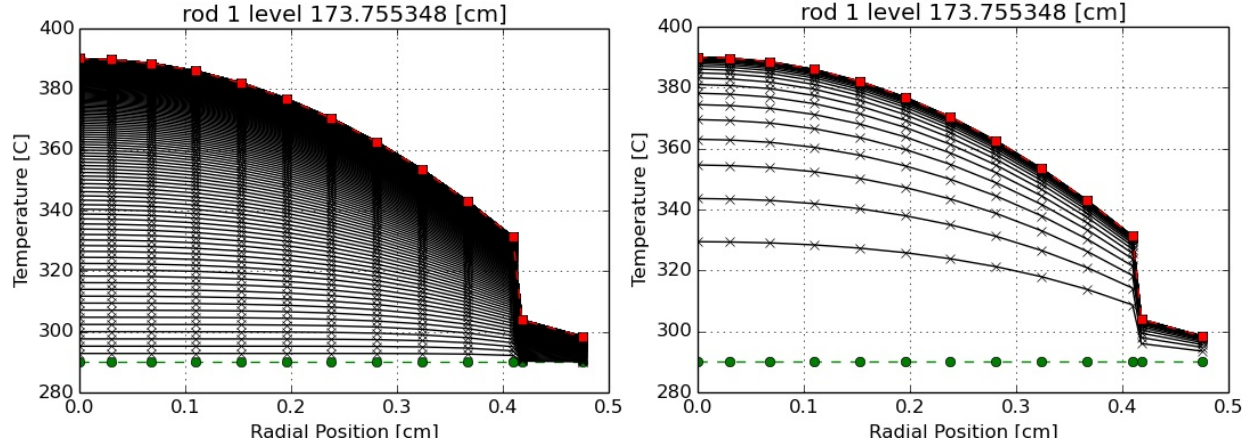


**Figure 8. Temperature profile over time for Semi-Implicit (left) and Implicit (right)**

#### 4. CONCLUSIONS

The residual formulation of the one-dimensional single-phase liquid and solid residual formulations were listed. Combining the liquid and solid equations into a single Jacobian matrix allowed for easy explicit or implicit coupling. This solution method was tested against the analytical solution for a single rod with uniform heat generation and shown to give good results. Future work will involve performing a more in depth verification analysis of the steady state and transient solutions. The effect of temperature dependent material properties and dynamic gap conductance will also be considered. A homogenous energy equation can now be easily implemented by adding the liquid and solid conservation equations. Future work will be analyzing the homogeneous energy approximation over a state space to see when the approximation is valid. Future work will also involve extending the conduction equations to azimuthal and axial directions.

## NOMENCLATURE

Symbol	Variable
$P$	Pressure
$h$	Enthalpy
$u$	Velocity
$\rho$	Density
$T$	Temperature
$t$	Time
$x$	Channel Axial Position
$r$	Rod Radial Position
$c_p$	Specific Heat
$k$	Thermal Conductivity
$q$	Heat Rate
$q'''$	Heat Generation Rate
$h_l$	Heat Transfer Coefficient
$\nabla$	Volume
A	Area
R	Thermal Resistance

## ACKNOWLEDGMENTS

This work has been supported by the Consortium for Advanced Simulation of Light water reactors, an Energy Innovation Hub for Modeling and Simulation of Nuclear Reactors under U.S. Department of Energy Contract No. DE-AC05-00OR22725.

## REFERENCES

1. R. K. Salko, "CTF Theory Manual", Penn State, (2014).
2. L. J. Lloyd, "Development of a Spatially-Selective, Nonlinear Refinement Algorithm for Thermal-Hydraulic Safety Analysis", The University of Wisconsin Madison, (2014).
3. J. R. Cooper and R. B. Dooley, "The International Association for the Properties of Water and Steam Revised Release on the IAPWS Industrial Formulation 1997 for the Thermodynamic Properties of Water and Steam," (2007).
4. Bergman, T. L., and Frank P. Incropera. *Fundamentals of Heat and Mass Transfer*. 6th ed. pp. 514, Hoboken, NJ (2007).
5. G.G. Botte, J.A. Ritter, and R.E. White, "Comparison of Finite Difference and Control Volume Methods for Solving Differential Equations", *Computers & Chemical Engineering* pp. 2633–